A Hybrid Causal Discovery Approach for Stability-Oriented Critical Contingency Selection

Amir Esmaeili-Nezhad
School of Electrical, Computer, and Energy Engineering
Arizona State University
Tempe, AZ, USA
aesmaei5@asu.edu

Reza Cheshomi
School of Electrical, Computer, and Energy Engineering
Arizona State University
Tempe, AZ, USA
reza_cheshomi@asu.edu

Mojdeh Khorsand
School of Electrical, Computer, and Energy Engineering
Arizona State University
Tempe, AZ, USA
mojdeh.khorsand@asu.edu

***Abstract*—Effective critical contingency selection in modern power systems requires identifying the true causal drivers underlying system responses to contingencies. However, most existing data-driven approaches remain limited by their reliance on correlation-based analysis, which can overlook critical mechanisms underlying system instability. To address this gap, this paper proposes a hybrid causal discovery approach that leverages complementary causal algorithms for robust structure learning, adaptation to nonstationarity, and orientation in nonlinear settings, enabling effective identification and prioritization of high-impact locations for transient stability risk. The results of case studies demonstrate that causality-based screening can reliably identify a small subset of critical buses and network corridors that account for the majority of instability risk. By focusing on causation rather than correlation, this approach offers enhanced interpretability, robustness, and operational value, and can pave the way for transitioning from black-box machine learning (ML) models to causality-aware, data-driven strategies in power system applications.**

***Index Terms*—Causal discovery, causal inference, contingency selection, feature selection, transient stability assessment.**

I. Introduction

Contingency analysis is a fundamental element of dynamic security assessment in modern power systems, protecting against violations of thermal and voltage limits as well as system-wide instability [1], [2]. To enhance the efficiency of contingency analysis, system operators typically prioritize and select a subset of critical contingencies for detailed simulation, a process widely referred to as contingency screening [3]. In operational practice, screening of stability-related contingencies—referred to as stability contingency screening—is particularly valuable to system planners, as these scenarios typically require substantially more computational effort to simulate compared to those involving only screening for thermal or voltage violations. When performing stability-oriented contingency analysis, the primary operational concern is rotor angle stability, due to its central importance in maintaining synchronous operation across the network [4].

Conventional contingency analysis methods, which rely on time-domain simulations of detailed dynamic models, are often computationally intensive and impractical for assessing a wide range of contingencies under changing operating scenarios [5], [6]. This computational burden limits their applicability in scenarios that require timely and informed decision-making. To overcome these challenges, recent research has explored data-driven and machine learning (ML) approaches for faster stability assessment and improved identification of critical contingencies. These methods typically leverage system measurements from phasor measurement units (PMUs) to train predictive models that evaluate transient stability without requiring full dynamic simulations. In the literature, various ML-based frameworks have been proposed to enhance the efficiency and accuracy of contingency selection and transient stability assessment. In [7], an online static security assessment approach based on artificial neural networks (ANNs) is proposed to estimate security indices for contingency screening and ranking. In [8], a deep neural network (DNN)-based method maps system states and topologies to prioritized contingency lists. However, both methods rely on conventional power flow calculations for input features. In [9], a deep convolutional neural network (CNN) is introduced to address unseen operating conditions and topological variations under N-1 contingencies. In [10], a CNN-based model with saliency maps is proposed for efficient identification of critical transient stability features, demonstrating robust performance even in noisy measurement scenarios.

Recent studies have also explored graph-based and spatial–temporal learning methods to capture the structural and dynamic characteristics of power systems. In [11], a comprehensive review highlights the effectiveness of graph neural networks (GNNs) in encoding network topology and modeling spatial and temporal correlations. Building on this, spatial–temporal learning-based frameworks have been introduced to improve transient stability assessment [12]–[15]. While these methods incorporate spatial–temporal information, they often lack adaptation for the unique complexities and nonlinear dynamics of transient stability analysis. In [16], a GNN-based technique is also introduced for detecting transient events using PMU data. However, this approach focuses primarily on predicting event stability rather than reconstructing the full system dynamic trajectories. In [17], a graph recurrent attention network (GRAN) is proposed to reconstruct bus trajectories using GNNs, but it assumes fixed and known network topology, which does not reflect actual operating conditions.

This work was supported by the U.S. Department of Energy (DOE) under Award No. DE-EE0011372.

979-8-3315-8138-1

While ML-based methods have improved the efficiency of transient stability assessment, most existing frameworks rely primarily on correlation for feature selection. Correlation describes a statistical association between variables but does not indicate whether one variable actually influences changes in another. As a result, conventional ML approaches may overlook or misinterpret the true mechanisms that drive system instability. Causality, in contrast, addresses how changes in one variable produce effects in another, thereby capturing the underlying mechanisms that correlation alone cannot expose. Thus, causality provides a deeper and more actionable understanding of power system dynamics by enabling the identification of true cause and effect relationships. By introducing the concept of causality into power system applications, the primary contributions of this paper are summarized as follows:

- A causality-aware contingency selection framework is introduced, employing a hybrid multi-stage causal discovery approach that combines constraint-based, nonstationary, and nonlinear learning algorithms to identify directional influences among system variables.
- A causal bus criticality index (BCI) is proposed as an interpretable metric for ranking bus locations according to their causal contribution to instability risk, enabling targeted and risk-informed contingency screening.
- By shifting the focus of data-driven frameworks from correlation to causation, this work advances the transition toward causality-aware contingency analysis, enabling greater interpretability, reliability, and operational value in power system security assessment.

II. Causal Discovery Framework

Figure 1 presents an overview of the proposed hybrid causal discovery framework. The framework begins with dataset generation, where post-fault dynamic measurements are collected and a comprehensive set of engineered features is extracted to characterize the critical electromechanical response of the system; it is worth noting that both historical data as well as results of offline simulations could be used in this stage. These features are organized into a scenario-feature matrix, where each scenario is labeled according to the computed stability margin. The engineered dataset is then analyzed using a multi-stage causal discovery process. The framework first applies the Peter-Clark (PC) algorithm [18] for robust structure identification, subsequently refines causal directions using the causal discovery from nonstationary or heterogeneous data (CD-NOD) algorithm [19], and finally employs the information geometric causal inference (IGCI) algorithm [20] to resolve orientation in nonlinear settings. Further details on each stage are provided in the following sub-sections.

A. Scenario Generation and Feature Engineering

Although historical measurement data—often collected without knowledge of the underlying generation mechanisms—can be utilized to construct samples for causal analysis, large disturbances and transient instability events are rare in actual power systems, resulting in a limited number of real-world examples. Thus, generating a comprehensive dataset through offline dynamic simulation is an effective way to address the scarcity of measured data for transient stability studies.

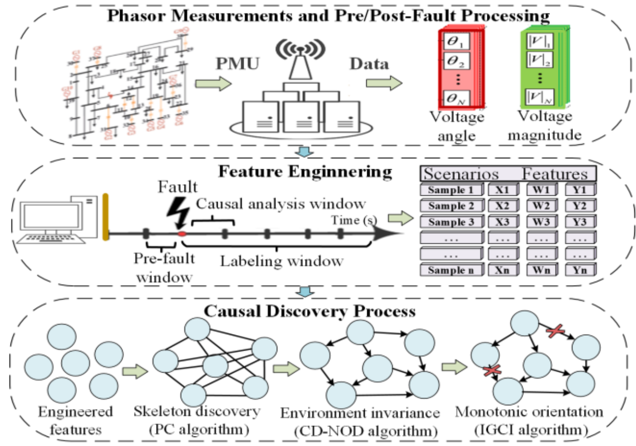

Fig. 1. Flowchart of the proposed hybrid causal discovery framework.

In this study, a dataset comprising 2,652 dynamic simulation scenarios is generated using the IEEE 39-bus test system, as illustrated in Fig. 2. System loads—both active and reactive—are uniformly scaled from 70% to 130% of their nominal values in 5% increments to represent a wide spectrum of operating conditions. For each power flow level, a set of three-phase short-circuit faults is assumed to occur at the end of each transmission line, with fault durations randomly selected from 0.08 s, 0.12 s, or 0.18 s. Faults are cleared by single line tripping (N-1), resulting in network topology changes. For each scenario, voltage phasors (magnitude and phase angle) are recorded for all buses with measurement frequency of 100 Hz, i.e., 10 ms, resulting in a time-series data array V of size $T \times B$:

$$V = \begin{bmatrix} V_{1,1} & \cdots & V_{1,B} \\ \vdots & \ddots & \vdots \\ V_{T,1} & \cdots & V_{T,B} \end{bmatrix} \tag{1}$$

where B is the number of buses and T is the number of time samples. All voltage phasor data are normalized using the mean and standard deviation computed over a 200 ms pre-fault steady-state window, ensuring that engineered features capture deviations from steady state and are comparable across scenarios. During the feature engineering process, a broad set of candidate post-fault features was evaluated, and the final set was selected for physical interpretability and relevance to dominant transient stability mechanisms. The selected features were also chosen to support consistent causal inference across the considered operating points and fault conditions within the modeled scenario space. The first feature, voltage dip (V_{dip}), captures the lowest value of normalized voltage recorded during the disturbance and is calculated as:

$$V_{dip} = \min_{t_{fault} \leq t \leq t_{end}} V_{norm}(t) \tag{2}$$

where $V_{norm}(t)$ is the normalized voltage magnitude, t_{fault} is the fault initiation time, and t_{end} is the end of the post-fault window. The second feature, voltage recovery ($V_{recovery}$), measures how quickly the voltage returns to its nominal value following fault clearance and is calculated as:

$$V_{recovery} = Slope(V_{norm}(t), t_{rec} \leq t \leq t_{end}) \tag{3}$$

where t_{rec} denotes the start time for evaluating voltage recovery. The third feature, angular swing energy ($\Delta\theta_{energy}$), reflects the total oscillatory energy and accumulated system stress during the disturbance and is determined by:

979-8-3315-8138-1

$$\Delta\theta_{energy} = \int_{t_{fault}}^{t_{end}} (\tilde{\theta}_j(t))^2 \, dt \tag{4}$$

where $\tilde{\theta}_j(t)$ denotes the normalized voltage angle at bus j (referenced to the network-average bus angle). The ground truth in this study is obtained based on the stability margin, denoted by η, which reflects the post-fault rotor angle dynamics. The stability margin is defined as follows:

$$\eta = \frac{180^{\circ} - |\Delta\delta|_{max}}{180^{\circ} + |\Delta\delta|_{max}} \tag{5}$$

where $|\Delta\delta|_{max}$ denotes the largest rotor angle difference observed throughout the simulation. If $|\Delta\delta|_{max} > 180°$ (i.e., $\eta \leq 0$), this indicates that one or more generators have lost synchronism, and the system is defined as unstable.

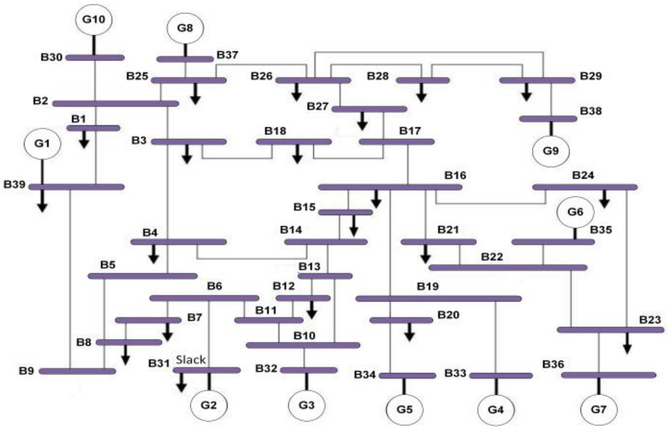

Fig. 2. Single-line diagram of the 39-bus benchmark system used in this study.

B. *Multi-Stage Causal Discovery Approach*

The proposed methodology leverages a multi-stage causal discovery framework to identify and quantify the most critical buses contributing to system-wide instability risk. As summarized in Algorithm 1, the PC algorithm is first applied to identify the causal skeleton by performing a series of conditional independence (CI) tests between variable pairs, as follows [18]–[20]:

$$\rho_{X,Y|k} = \frac{\rho_{X,Y|k\setminus\{h\}} - \rho_{X,h|k\setminus\{h\}}\,\rho_{Y,h|k\setminus\{h\}}}{\sqrt{(1-{\rho^2}_{X,h|k\setminus\{h\}})(1-{\rho^2}_{Y,h|k\setminus\{h\}})}} \, , h \in k \tag{6}$$

where $\rho_{X,Y|k}$ is the partial correlation between variables X and Yconditioned on the set k, h denotes an arbitrary element in k ($h \in k$), and $k \setminus \{h\}$ denotes the conditioning set with h removed. This value is then transformed using a Fisher Z transformation as follows [18]:

$$Z(X,Y|k) = \frac{1}{2} \, ln \, (\frac{1+\hat{\rho}_{X,Y|k}}{1-\hat{\rho}_{X,Y|k}}) \tag{7}$$

where $\hat{\rho}_{X,Y|k}$ denotes the sample estimate. A hypothesis test at significance level $\alpha \in (0,1)$ is conducted to determine whether X and Y are conditionally independent given k as follows:

$$\left[\sqrt{n-|k|-3}\right] |Z(X,Y|k)| \leq \Phi^{-1}(1-\frac{\alpha}{2}) \tag{8}$$

where n is the sample size, and Φ is the standard normal cumulative distribution function. In the context of power systems, a CI test might evaluate whether the voltage dip feature at bus X is conditionally independent of the angular swing energy feature at bus Y, given a conditioning subset of other features. In this study, edge orientation refers to assigning a causal direction to an undirected adjacency (e.g., $X \rightarrow Y$ versus $Y \rightarrow X$). The inferred structure is then oriented using two complementary approaches. First, the CD-NOD algorithm orients edges by leveraging distributional shifts across multiple environments. The underlying principle is that the conditional distribution of an effect given its cause (the causal mechanism) remains invariant across environments. Therefore, if the conditional distribution $P(Y \mid X)$ is observed to be stable across environments while $P(X \mid Y)$ varies, the algorithm infers the causal direction $X \rightarrow Y$. Second, the IGCI algorithm is applied to orient the remaining undirected adjacencies by exploiting asymmetries in nonlinear functional relationships under the independence of cause and mechanism (ICM) assumption, as described in [20]. In the final step, directed feature-level causal influences are systematically mapped to their corresponding bus locations, producing a raw importance score denoted as r_b. These scores are then normalized to obtain the BCI for each bus as follows:

$$c_b = \frac{r_b}{\sum_{j\in B} r_j}, \qquad \sum_b c_b = 1 \tag{9}$$

where B is the set of all buses, and c_b is the normalized BCI value for bus b. It is important to note that BCI is a causal metric, fundamentally distinct from probability-based or frequency-based indices. The BCI is calculated across all stable and unstable scenarios, as the inclusion of stable cases provides essential counterfactual contrast that enables the causal discovery algorithms to isolate true causal effects. In addition, BCI does not simply count unstable events. Instead, it quantifies the causal influence of each bus on the emergence or prevention of instability, regardless of fault location, thereby capturing the true system-wide impact of each location.

Algorithm 1: Multi-Stage Causal Discovery Algorithm.

1. **Require**:
   - Normalized engineered feature matrix $\boldsymbol{\chi}$;
   - PC parameters (conditional independence (CI) test, significance level $\boldsymbol{\alpha}$, max conditioning set size $\boldsymbol{L}$);
2. **Step 1:** Initial causal skeleton discovery (PC algorithm)
   - Apply the PC algorithm to $\boldsymbol{\chi}$ to construct a causal skeleton $\boldsymbol{\mathcal{G}}$.
3. **Step 2:** Environment-based invariance testing (CD-NOD)
   - Apply invariance tests for all unshielded triples and edges across environments to orient edges in $\boldsymbol{\mathcal{G}}$.
4. **Step 3:** Nonlinear monotonicity enhancement (IGCI)
   - Apply the IGCI algorithm to resolve edge directions for remaining ambiguous feature pairs in $\boldsymbol{\mathcal{G}}$.
5. **Step 4:** Bus-level causal importance scoring
   - Map directed feature-level edges in $\boldsymbol{\mathcal{G}}$ to corresponding bus locations;
   - For each bus, aggregate the causal influence scores to obtain bus-level causal importance values $\{\boldsymbol{r_b}\}$ for each bus $\boldsymbol{b}$.
6. **Step 5:** Normalization and ranking
   - For each bus, normalize the raw scores to obtain $\boldsymbol{c_b}$;
   - Rank buses by their $\boldsymbol{c_b}$ to obtain the final bus-level causal importance.

Return: $\{\boldsymbol{c_b}\}$ — normalized BCI.

III. EVALUATION AND INTERPRETATION

Figures 3 and 4 summarize the results of the proposed causal discovery framework for the IEEE 39-bus system, revealing that system-wide instability risk is non-uniformly distributed

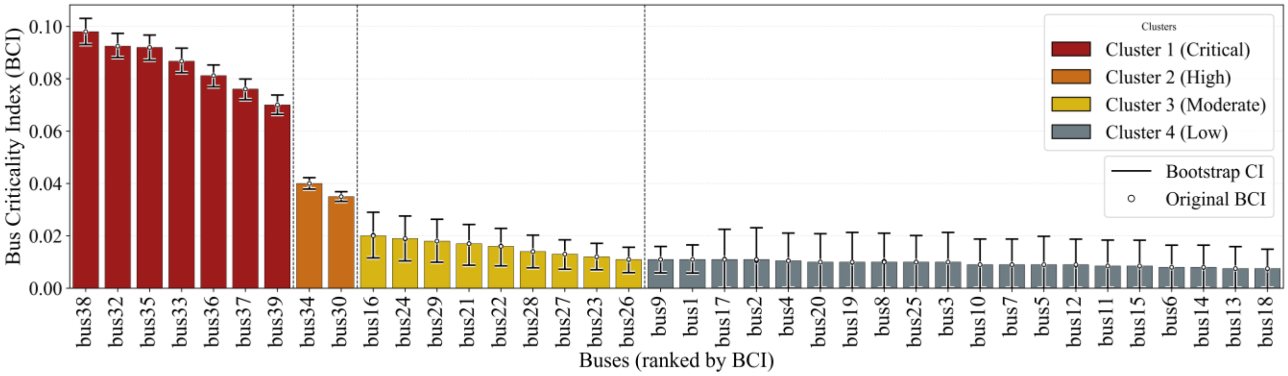

Fig. 3. Causal bus importance scores, indicating the contribution of each bus to system-wide instability risk.

and concentrated among a small subset of critical locations. Figure 3 presents the detailed BCI rankings, along with their statistical validation. The results confirm that BCI rankings are consistent with the underlying system topology, with bus locations grouped into four clusters based on their BCI values. Clusters 1 and 2 (Critical and High) are dominated by generator terminal buses, identifying their primary causal role in instability. Cluster 3 (Moderate) includes key nodes along major inter-area transfer corridors, such as buses 16, 24, and 29, which serve as primary electrical boundaries where large angle separations are likely to develop. In contrast, Cluster 4 (Low) predominantly includes interior load buses, confirming their limited causal contribution. These buses are characterized by much smaller and more variable BCI scores, reflecting their comparatively limited influence on system-wide instability events. The statistical robustness of the causal importance ranking is validated by bootstrap confidence intervals, also shown in Fig. 3. This analysis, conducted with 200 resampled scenarios, quantifies the variability in BCI values. The small, non-overlapping error bars associated with the high-BCI buses in Clusters 1 and 2 indicate that their rankings are statistically robust and not an artifact of random data variations. Figure 4 quantitatively aggregates these results, illustrating the total instability risk contributed by each cluster. Cluster 1, which contains only 7 buses, accounts for nearly 60% of the total system risk. In contrast, Clusters 3 and 4, which together comprise 29 buses (the majority of the system), contribute only about 33% of the total risk. These results validate the BCI as an interpretable and reliable metric for identifying high-impact locations. These insights support the transition from uniform resource allocation to a highly targeted, risk-informed strategy, allowing operators to focus screening and mitigation efforts on the small subset of high-BCI locations, thereby enhancing the overall effectiveness of system security management.

Figure 5 presents the cumulative coverage of system instability risk as buses are incrementally screened based on their BCI values, with the top x-axis indicating the ranking order of buses according to their causal criticality. This dual-axis format visualizes the efficiency of the causality-based ranking and provides immediate insight into the physical locations in the network prioritized by the proposed methodology. The results demonstrate that the causality-based ranking is highly effective, capturing a large portion of system instability risk by screening only the most critical subset of buses. The nonlinear shape of the cumulative risk curve demonstrates that system-wide instability risk is non-uniformly distributed and concentrated within a small subset of high-impact locations. This approach enables a more computationally efficient and targeted contingency analysis by prioritizing critical buses, thereby reducing the scope of detailed assessment required for effective system stability management. For instance, selecting the top 7 buses based on the BCI captures approximately 60% of the total instability risk. Expanding the screening set to the top 9 and 18 buses increases the coverage to 67% and 81%, respectively. Overall, these findings support causality-based screening as an effective tool for critical contingency selection and support the adoption of interpretable, causality-aware approaches alongside traditional black-box correlation-based methods [21]. In particular, incorporating causality provides a physically grounded and interpretable basis for prioritization by identifying key factors that are consistently linked to critical contingencies.

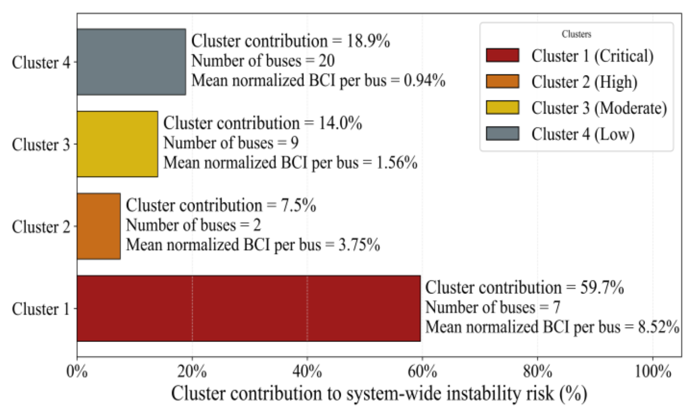

Fig. 4. Contribution of each cluster to system-wide instability risk.

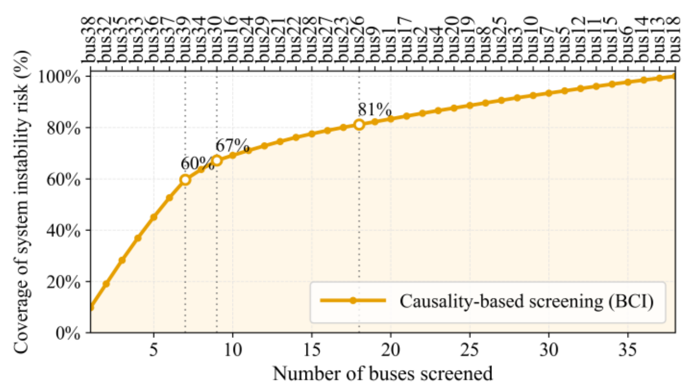

Fig. 5. Instability risk coverage as a function of the number of buses selected by the causality-based (BCI) screening method.

979-8-3315-8138-1

To validate the effectiveness of the proposed causal discovery framework against a classical ground truth, Fig. 6 shows generator rotor angle trajectories for two representative contingencies. In the scenario illustrated in Fig. 6(a), a three-phase fault applied at the end of the transmission line between Buses 13 and 14 leads to only minor deviations in post-fault rotor angles, with all generators rapidly resynchronizing, which is indicative of a stable system response. This is consistent with the causal discovery results, as this location is not identified as critical. In contrast, Fig. 6(b) presents the system response to a fault at the end of the line connecting Buses 28 and 29, which is located on a network corridor identified by the causal analysis as high risk. In this case, even with a shorter fault duration, one generator rotor angle diverges continuously from the other generators after fault clearing, indicating loss of synchronism and transient instability. These results are consistent with the time-domain instability criterion and further support the validity of the causal discovery results. It should be emphasized that for large-scale grids, the proposed framework can be applied in parallel over regional or coherency-based subareas by reducing the causal search space using network topology or electrical distance, and then aggregating the resulting bus-level criticality scores across areas.

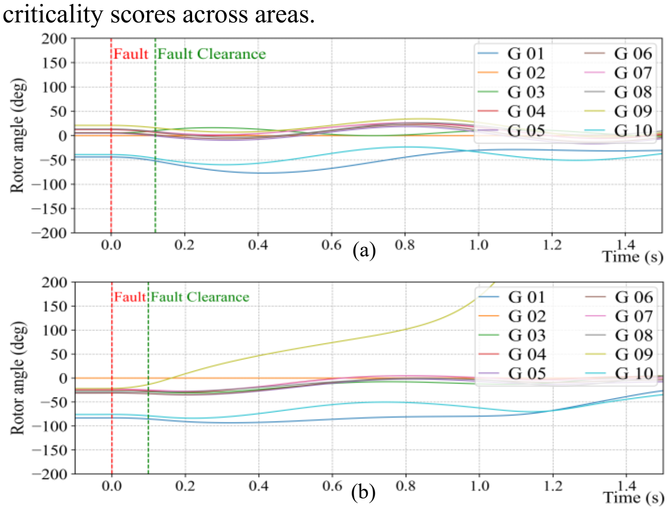

Fig. 6. Rotor angle trajectories for two representative scenarios: (a) stable and (b) unstable.

IV. Conclusion

This paper presents a novel hybrid causal discovery framework for critical contingency selection and transient stability risk assessment. By integrating causal inference with engineered post-fault features, the proposed method introduces the BCI, a robust and interpretable metric for quantifying causal contributions to system instability. The validity of the BCI is supported by its statistical robustness under bootstrap resampling, its alignment with the physical topology as reflected in the prioritization of generator terminals and major transfer corridors, and its agreement with time-domain simulation results. Case studies on the IEEE 39-bus system show that instability risk is concentrated in the small subset of buses and corridors identified by the BCI. These findings highlight the practical value of causality-aware screening for more efficient and targeted stability analysis. Future work will validate scalability on larger systems, extend the contingency set to include N-1-1 and N-2 events, and explore using BCI as an interpretable input to ML-based models, particularly for grids with high renewable integration, to further advance actionable tools for power system security.

References

[1] G. Lu and S. Bu, “Adaptive stability contingency screening for operational planning based on domain-adversarial graph neural network,” *IEEE Trans. Power Syst.*, vol. 39, no. 1, pp. 1503–1516, 2024.

[2] C. Shen, K. Zuo, and M. Sun, “Physics-following neural network for online dynamic security assessment,” *IEEE Trans. Power Syst.*, vol. 40, no. 6, pp. 4746–4759, 2025.

[3] J. Hu, Q. Wang, Y. Ye, Z. Wu, and Y. Tang, “A high temporal–spatial resolution power system state estimation method for online DSA,” *IEEE Trans. Power Syst.*, vol. 39, no. 1, pp. 877–889, Jan. 2024.

[4] C. Ren, Y. Xu, and R. Zhang, “An interpretable deep learning method for power system transient stability assessment via tree regularization,” *IEEE Trans. Power Syst.*, vol. 37, no. 5, pp. 3359–3369, 2022.

[5] S. Naderi, M. Javadi, M. Mazhari, and C. Y. Chung, “A machine learning-based framework for fast prediction of wide-area remedial control actions in interconnected power systems,” *IEEE Trans. Power Syst.*, vol. 38, no. 1, pp. 242–255, Jan. 2023.

[6] S. Naderi, M. Javadi, M. Mazhari, and C. Y. Chung, “Data-driven approach for generator rejection prediction to prevent transient instability in power system using wide-area measurements,” *IEEE Access*, vol. 10, pp. 96748–96759, 2022.

[7] R. Sunitha, R. S. Kumar, and A. T. Mathew, “Online static security assessment module using artificial neural networks,” *IEEE Trans. Power Syst.*, vol. 28, no. 4, pp. 4328–4335, Nov. 2013.

[8] T. Ibrahim and A. Mohamed, “DNN-based contingency screening module for voltage stability analysis,” *in Proc. North Amer. Power Symp. (NAPS)*, 2019, pp. 1–6.

[9] Y. Du, F. Li, T. Zheng, and J. Li, “Fast cascading outage screening based on deep convolutional neural network and depth-first search,” *IEEE Trans. Power Syst.*, vol. 35, no. 4, pp. 2704–2715, Jul. 2020.

[10] H. Lee, J. Kim, J. H. Park, and S.-H. Chung, “Power system transient stability assessment using convolutional neural network and saliency map,” *Energies*, vol. 16, no. 23, p. 7743, 2023.

[11] W. Liao, B. Bak-Jensen, J. R. Pillai, Y. Wang, and Y. Wang, “A review of graph neural networks and their applications in power systems,” *J. Mod. Power Syst. Clean Energy*, vol. 10, no. 2, pp. 345–360, 2022.

[12] J. Huang, L. Guan, Y. Su, H. Yao, M. Guo, and Z. Zhong, “Recurrent graph convolutional network-based multi-task transient stability assessment framework in power system,” *IEEE Access*, vol. 8, pp. 93283–93296, 2020.

[13] J. Huang, L. Guan, Y. Su, H. Yao, M. Guo, and Z. Zhong, “System-scale-free transient contingency screening scheme based on steady-state information: A pooling-ensemble multi-graph learning approach,” *IEEE Trans. Power Syst.*, vol. 37, no. 1, pp. 294–305, Jan. 2022

[14] L. Zhu and D. Hill, “Networked time series shapelet learning for power system transient stability assessment,” *IEEE Trans. Power Syst.*, vol. 37, no. 1, pp. 416–428, Jan. 2022.

[15] L. Zhu and J. Lin, “Learning spatiotemporal correlations for missing noisy PMU data correction in smart grid,” *IEEE Internet Things J.*, vol. 8, no. 9, pp. 7589–7599, May 2021.

[16] Y. Yuan, Z. Wang, and Y. Wang, “Learning latent interactions for event classification via graph neural networks and PMU data,” *IEEE Trans. Power Syst.*, vol. 38, pp. 617–629, Jan. 2023.

[17] J. Q. Yu, D. J. Hill, V. O. K. Li, and Y. Hou, “Synchrophasor recovery and prediction: A graph-based deep learning approach,” *IEEE Internet Things J.*, vol. 6, no. 5, pp. 7348–7359, Oct. 2019.

[18] M. Kalisch and P. Bühlmann, “Estimating high-dimensional directed acyclic graphs with the PC-algorithm,” *J. Mach. Learn. Res.*, vol. 8, pp. 613–636, May 2007.

[19] B. Huang, K. Zhang, J. Zhang, et al., “Causal discovery from heterogeneous/nonstationary data,” *J. Mach. Learn. Res.*, pp.1–53, 2020.

[20] D. Janzing, J. Mooij, K. Zhang, et al., “Information-geometric approach to inferring causal directions,” *Artif. Intell.*, pp. 1–31, 2012.

[21] A. Esmaeili-Nezhad, R. Cheshomi, and M. Khorsand, “A causality-oriented neural network framework for transient stability prediction in power systems,” in *Proc. 59th Hawaii Int. Conf. Syst. Sci. (HICSS)*, 2026, pp. 3240–3249.

979-8-3315-8138-1